## **ChemComm**



## COMMUNICATION

View Article Online



Cite this: *Chem. Commun.*, 2018, 54, 14120

Received 30th August 2018, Accepted 14th November 2018

DOI: 10.1039/c8cc07026a

rsc.li/chemcomm



A novel and efficient method is demonstrated to improve the electrochemical performance of  $\text{Li}_4\text{Ti}_5\text{O}_{12}$  and metal-oxide anodes. In contrast to other methods, inexpensive red phosphorus powder is used as a reducing reagent, and the reduction is conducted at a relatively low temperature of 400 °C. This method offers a low cost and effective way for  $\text{Li}_4\text{Ti}_5\text{O}_{12}$  and metal-oxide anode applications.

Lithium-ion batteries have been applied in various portable electronic devices and recently considered as an ideal energy device for electric vehicles. The current commercial Li ion battery composed of a transitional-metal oxide cathode and graphite anode cannot meet the demands of these vehicles due to the poor rate capability and safety issues (dendritic lithium) of the graphite anode. Li<sub>4</sub>Ti<sub>5</sub>O<sub>12</sub> (LTO) is used to replace graphite because it is lithium dendrite free and shows a long cycle life as a result of its minimal lattice expansion (less than 1%) during the charge/discharge process. However, its intrinsically poor electronic conductivity has restricted LTO from showing high rate performance. Many approaches have been used to increase the electronic conductivity of LTO, 1-11 which can be categorized into the following three ways: (i) preparation of LTO small-particles

There are two main ways to reduce Ti<sup>4+</sup> in LTO to Ti<sup>3+</sup>. One method is done by using a transition metal, such as Cr, Mo, Cu, Co, or Ta, to partially replace Li or Ti in the lattice, <sup>12-18</sup> and another approach is to use reducing reagents. <sup>19</sup> Almost all the reported methods require high temperature (higher than 600 °C), <sup>12-19</sup> which limits the application of these approaches.

In this work, we present a novel method to reduce Ti<sup>4+</sup> in LTO to Ti<sup>3+</sup> using red phosphorus powder as a reducing reagent, which can sublime at a relatively low temperature (400 °C). When LTO and a trace amount of phosphorous powder were mixed and sintered at about 400 °C, the red phosphorus sublimed, taking away O in the LTO nanoparticle, forming oxygen vacancies in the LTO lattice. X-ray diffraction (XRD), X-ray photoelectron spectroscopy (XPS), and electron paramagnetic resonance (EPR) are employed to examine the change in Ti after phosphorus treatment. Scanning electron microscopy (SEM) reveals that the reduction does not change the morphology of the LTO sample, and high-resolution transmission electron microscopy (HRTEM) shows that the LTO after reduction maintains high crystallinity. The phosphorus treated LTO/P electrode demonstrates greatly improved performance in terms of capacity, rate, and cycling capability when compared to the non-treated LTO electrode. Cyclic voltammetry at different scan rates and EIS results disclose that both Li<sup>+</sup> diffusion and electronic diffusion are enhanced for the LTO/P electrode. This simple, inexpensive, and efficient method can also be expanded to improve the electrochemical performance of other metal-oxide anode materials such as MoO<sub>3</sub>.

LTO was synthesized via a solid-state reaction at 800 °C. <sup>4</sup> 1 wt% red phosphorus powder was used as the reduction reagent to modify LTO and the oxidation product of red phosphorus ( $P_2O_5$ ) sublimed at 360 °C. The non-modified LTO was a white powder (Fig. 1a, inset) and the ground red phosphorus LTO sample (LTO + P) was pink colored (Fig. 1a, inset),

with various morphologies, (ii) coating the surface of LTO with carbon or other conductive agents and (iii) reducing Ti<sup>4+</sup> to more conductive Ti<sup>3+</sup>. Among them, the reduction of LTO is considered to be the most favorable method for practical applications.<sup>6</sup>

There are two main ways to reduce Ti<sup>4+</sup> in LTO to Ti<sup>3+</sup>

<sup>&</sup>lt;sup>a</sup> Institute of Materials Science and Devices, Suzhou University of Science and Technology, Suzhou 215000, P. R. China

b Department of Chemistry and Biochemistry, Florida State University, Tallahassee, Florida 32306, USA. E-mail: hu@chem.fsu.edu

<sup>&</sup>lt;sup>c</sup> National High Magnetic Field Laboratory, 1800 East Paul Dirac Drive, Tallahassee, FL 32310, USA

<sup>&</sup>lt;sup>d</sup> Anhui Province Key Laboratory of Condensed Matter Physics at Extreme Conditions, High Magnetic Field Laboratory of Chinese Academy of Sciences, Hefei 230031. P. R. China

<sup>&</sup>lt;sup>e</sup> College of Chemistry and Molecular Sciences, Wuhan University, Wuhan 430072, China

<sup>&</sup>lt;sup>f</sup>Department of Applied Biology and Chemical Technology, The Hong Kong Polytechnic University, Hung Hom, Hong Kong, P. R. China

g Institute for Clean Energy & Advanced Materials, Southwest University, Chongqing 400715, P. R. China. E-mail: ecmli@swu.edu.cn

<sup>†</sup> Electronic supplementary information (ESI) available: Experimental details, SEM, TEM, EDS results and XPS results of <sup>31</sup>P, XRD patterns of P, and EPR spectra of the LTO and LTO/P samples. See DOI: 10.1039/c8cc07026a

<sup>‡</sup> The authors contributed equally to this work.

Communication ChemComm

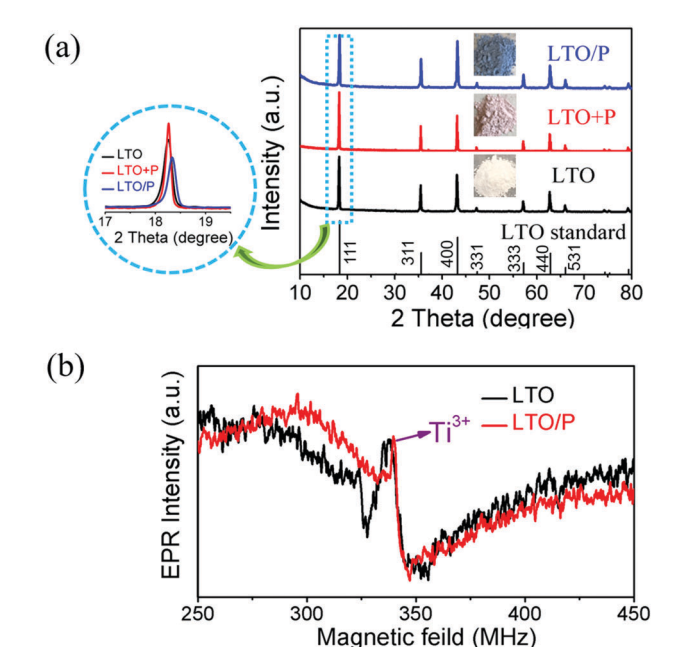


Fig. 1 (a) XRD patterns of the LTO, LTO + P, and LTO/P samples. (b) electron spin resonance spectra of the LTO and LTO/P samples recorded at 140 K.

while the color of the LTO/P sample turned blue (Fig. 1a, inset), which is a typical signal for the appearance of Ti3+ and oxygen vacancies in LTO. 12,20 Fig. 1(a) shows the XRD patterns of the LTO, LTO + P and LTO/P samples. It can be observed that all XRD peaks for these three samples are sharp, which implies their high crystallinity. Moreover, all these diffraction peaks are well indexed to a cubic spinel structure of Li<sub>4</sub>Ti<sub>5</sub>O<sub>12</sub> (space group: Fd3m, JCPDS, No. 49-0207). No diffraction peaks for red phosphorous (Fig. S1, ESI†) can be found from LTO + P, since red phosphorous is amorphous and the amount is low. However, upon zooming in on the peak that is attributed to the 111 planes, we can observe that the diffraction angle  $(2\theta)$  increases slightly for the LTO/P sample (18.34° for pristine LTO and LTO + P, 18.45° for LTO/P). On the basis of Bragg's equation, the higher diffraction angle means a smaller lattice parameter, which is probably due to the reduction of Ti<sup>4+</sup> to Ti<sup>3+</sup> and the generated oxygen vacancies.<sup>6</sup>

To confirm the existence of Ti<sup>3+</sup>, XPS and EPR characterization experiments were performed. The XPS results (Ti 2p spectra) for the pristine LTO and LTO/P samples were compared and shown in Fig. S2 (ESI†). As can be seen, two new peaks at 463.1 and 457.3 eV, which are the characteristic peaks of Ti<sup>3+</sup> appeared for the LTO/P sample, suggesting the potential reduction of Ti<sup>4+</sup> to Ti<sup>3+</sup>. EPR measurements were conducted at 140 K in order to further prove the existence of Ti<sup>3+</sup>. As can be seen in Fig. 1b, a peak at 332 MHz appeared for the LTO/P sample, and according to Shiraishi et al., 21 it can be ascribed to  $Ti^{3+}$  ( $g = 0.07145 \times \gamma \text{ (MHz)/}H \text{ (mT)} = 1.98$ ), again confirming the potential reduction of Ti<sup>4+</sup> to Ti<sup>3+</sup> in the LTO lattice after phosphorus treatment. Furthermore, we examined the EPR spectrum for the LTO/P sample at room temperature to see whether there are signals for oxygen vacancies. As can be seen in Fig. S3 (ESI $\dagger$ ), three signals appear at g = 2.038, 2.008, and 1.975,

which should be attributed to the single electron trapped in the oxygen vacancies according to ref. 22.

The morphology of the LTO powder before and after phosphorus treatment was characterized by SEM and TEM. The SEM image in Fig. S4 (ESI†) shows that LTO possesses submicron sized particles connected to form a percolated network, and the high magnification SEM image shows that the surface of LTO is rough (Fig. S2b, ESI†). For the LTO/P particles, the morphology is extremely similar to that of LTO, indicating that the phosphorus reduction did not disturb the basic morphology of LTO. The TEM images show that the LTO and LTO/P nanoparticles have particle sizes ranging from 30 to 100 nm (Fig. S5a and d, ESI†). The HRTEM images (Fig. S5b, c and e, f, ESI†) reveal that both LTO and LTO/P samples are highly crystalline with a spinel structure. Energy dispersive X-ray spectroscopy (EDS) mapping analysis (Fig. S6, ESI†) shows that the LTO/P sample contains about 0.48 wt% phosphorus, which is less than that in LTO + P and this means that P gets evaporated partly in the form of P<sub>2</sub>O<sub>5</sub>. XPS was used to analyze the oxidation state of P<sub>2p</sub> in the LTO/P sample. As shown in Fig. S7 (ESI†), the peak located at  $\sim 133$  eV is assigned to metal phosphate, which is most probably Li<sub>3</sub>PO<sub>4</sub>, implying that the red phosphorus was oxidized from 0 to +5 valences and reacted with excess Li from the pristine LTO. Since only 1 wt% red phosphorus powder was used, the amount of Li<sub>3</sub>PO<sub>4</sub> formed on the surface of LTO/P is negligible. Li<sub>3</sub>PO<sub>4</sub> is ionically conductive, which might help improve the ion diffusion between the electrolyte and the electrode, and thus improve the electrochemical performance.

Fig. 2 shows the electrochemical performance of the LTO and LTO/P electrodes. As can be seen from Fig. 2a and b, when cycled at 0.2C (1C = 170 mA g<sup>-1</sup>), the LTO and LTO/P electrodes delivered a capacity of 165 and 170 mA h g<sup>-1</sup>, respectively. Meanwhile, the LTO/P electrode showed lower hysteresis  $(\Delta V, \text{Fig. 2b})$  than the LTO electrode (Fig. 2a). With the increase of the current density, the overpotential of the LTO electrode increased dramatically, while that of the LTO/P electrode

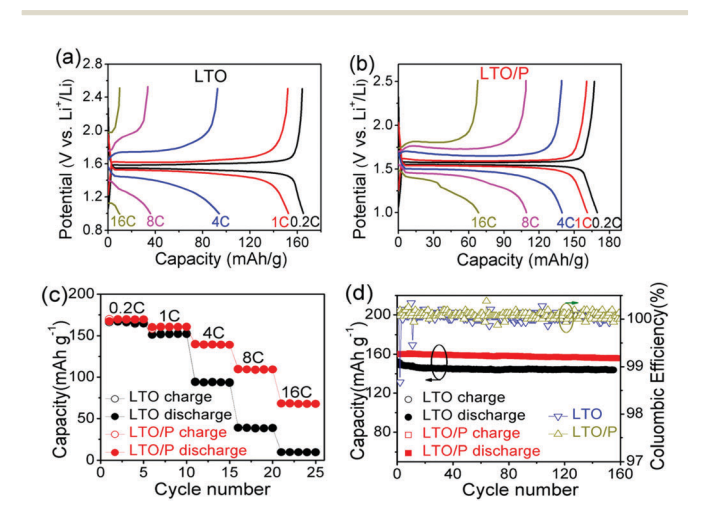


Fig. 2 Charging/discharging profiles at different rates for LTO (a) and LTO/P (b) electrodes; (c) cycling stability of LTO and LTO/P electrodes at different rates; (d) cycling stability of LTO and LTO/P electrodes at 1C.

ChemComm Communication

increased slowly, indicating smaller polarization for the LTO/P electrode during charging/discharging. It is observed that two discharge plateaus appear at 16C in Fig. 2b, which are attributed to different Li insertion processes. Normally, Li<sup>+</sup> from site 8a would transfer to site 16c during discharging, however, at a high discharge rate, this transfer might not happen, leading to a different plateau. We discussed this phenomenon in our previous works.<sup>4,9</sup> Furthermore, as can be seen from Fig. 2c, when the rate increased to 4C, the capacity of the LTO electrode decreased rapidly to 100 mA h g<sup>-1</sup>, while the LTO/P electrode still maintained a capacity of 140 mA h g<sup>-1</sup>. Even at a rate of 16C, the LTO/P electrode can still deliver a capacity of 75 mA h g<sup>-1</sup>, which is very promising for high-rate applications of LTO. Moreover, the LTO/P electrode demonstrates a much better cycling stability than the pristine LTO electrode. As can be seen in Fig. 2d, after being cycled at 1C for 160 times, the LTO electrode maintained a capacity of 140 mA h g<sup>-1</sup>, while the LTO/P electrode maintained a capacity of 156 mA h g<sup>-1</sup>, corresponding to a capacity retention of 96%, which is advantageous compared with the capacity retention of the pristine LTO electrode (90%). The superior electrochemical performance of the LTO/P electrode should be attributed to the oxygen vacancies and Ti3+ created by phosphorus reduction, because it has been reported that oxygen vacancies and Ti<sup>3+</sup> could enhance the electrical conductivity and lithium storage properties of the LTO electrode. 20,23,24

To better understand the reason why phosphorus reduction enhanced the electrochemical performance of LTO, we conducted CV and EIS analysis. Fig. 3a and b show the CV test for the LTO and LTO/P electrodes at different scan rates (from 0.2 to 0.8 mV s<sup>-1</sup>). As can be observed, the CV profiles for the LTO and LTO/P electrodes are similar. To clearly illustrate the difference, the peak current  $i_{\rm p}$  (mA) for cathodic and anodic scans is plotted against the square root of the scanning rate  $((V s^{-1})^{1/2})$  as presented in Fig. 3c and d. For faradaic processes,  $i_p$  and  $v^{1/2}$  are linearly correlated.<sup>4</sup>

$$i_{\rm p} = (2.69 \times 10^5) n^{3/2} A D_{\rm Li} + {}^{1/2} C_{\rm Li} + {}^{1/2}$$
 (1)

where n is the number of electrons involved on each charge carrier  $(n = 1 \text{ for Li}^+)$ ,  $A \text{ (cm}^2)$  is the surface area of the electrode,  $C_{\text{Li}^+}$  (moles per cm<sup>3</sup>) is the bulk concentration of Li<sup>+</sup> (0.03) and  $D_{\text{Li}^+}$  (cm<sup>2</sup> s<sup>-1</sup>) is the Li<sup>+</sup> diffusivity. According to eqn (1), the calculated  $D_{\mathrm{Li}^+}$  values for the LTO and LTO/P electrodes at the cathodic scan are  $3.69 \times 10^{-13}$  and  $4.73 \times 10^{-13}$  cm<sup>2</sup> s<sup>-1</sup>, respectively. While at the anodic scan, the  $D_{L,i^+}$  values for these two electrodes are  $2.84 \times 10^{-13}$  and  $3.68 \times 10^{-13}$  cm<sup>2</sup> s<sup>-1</sup>, respectively. This suggests that, during charging and discharging, the LTO/P electrode demonstrates a slightly higher  $D_{Li^+}$  than the LTO electrode. EIS was performed for the LTO and LTO/P electrodes. The AC impedance spectra are fitted with two different equivalent circuits as shown in the insets in Fig. 3e and f. After the 1st cycle, an obvious semicircle can be seen for both LTO and LTO/P electrodes. An intercept at the Z' real axis in the high frequency represents the resistance of the electrolytes  $(R_s)$ , while the semicircles ending at frequencies of 40 Hz and 158 Hz, respectively, are characteristics of charge transfer resistance ( $R_{ct}$ ). After the 20th cycle, two semicircles appear for both samples, in which the semicircle in the high frequency region corresponding to  $R_1$  is

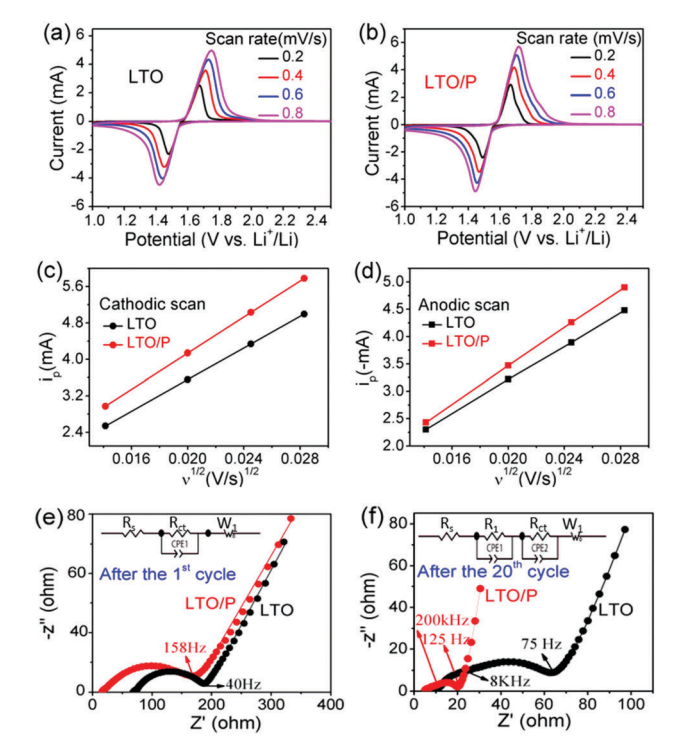


Fig. 3 Cyclic voltammetry of half-cell batteries employing (a) the LTO and (b) LTO/P electrodes; a plot of the peak current  $i_p$  vs. the square root of the voltage scanning rate for the LTO and LTO/P electrodes at (c) cathodic and (d) anodic scans; the fitted Nyquist plots of the LTO and LTO/P electrodes (e) after the 1st cycle and (f) after 20 cycles, frequency range: 0.1 Hz to  $5 \times 10^{6} \text{ Hz}.$ 

characteristic of the surface film formed on the electrodes, 25 while the semicircle in the low frequency region is characteristic of the charge transfer resistance  $(R_{ct})$  related to the lithium ion interfacial charge transfer. The relatively high  $R_{ct}$  for both samples at the beginning (1st cycle) is due to the bad wetting between the electrolyte and the electrode. Further, Fig. 3e shows that LTO/P has a lower  $R_s$  value than LTO, indicating that the former shows better wettability than the latter and it can be ascribed to the existence of Ti<sup>3+</sup> in the former, which improved the conductivity. After 20 cycles, the resistance of both samples decreases to less than 100 ohms, which may be due to the wetting of the electrodes after cycling that promoted the Li<sup>+</sup> diffusion. After 20 cycles, the wettability of both electrodes became better, so the  $R_s$  decreased and got close. It can be noticed in Fig. 3f that the  $R_{ct}$  for LTO/P (10  $\Omega$ ) is about 1/5 of that of the LTO electrode (50  $\Omega$ ), indicating a sharply decreased interfacial resistance for the fast charge transfer process of the phosphorus treated sample during charging/ discharging due to more Ti<sup>3+</sup> in the LTO/P sample.<sup>6,13</sup> Therefore, it can be concluded that more Ti3+ in LTO/P is not only beneficial for the charge transfer process, but also can reduce the R<sub>s</sub>. What's more, the overall electrode resistance  $(R_1 + R_{ct})$  of LTO/P (15  $\Omega$ ) is 3 times less than that of the LTO electrode (60  $\Omega$ ), resulting in better rate performance.

Phosphorus reduction was also conducted on MoO3 to partially reduce Mo6+ and test its effect on the metal oxide electrode. MoO3 was mixed with 1 wt% red phosphorus powder Communication ChemComm

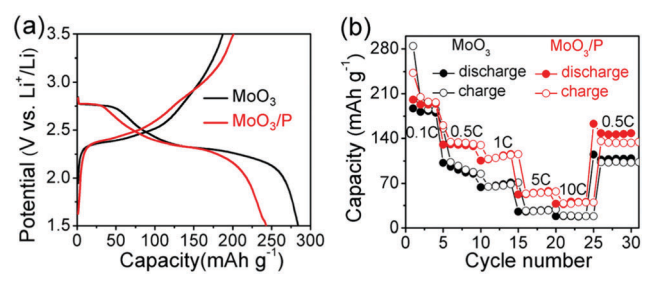


Fig. 4 (a) Charging/discharging profiles for the MoO<sub>3</sub> and MoO<sub>3</sub>/P electrodes at 0.1C (1C = 300 mA h  $g^{-1}$ ); (b) cycling of the MoO<sub>3</sub> and MoO<sub>3</sub>/P electrodes at different rates.

and sintered under vacuum at 400 °C for 2 h. The electrochemical performance of the MoO<sub>3</sub> and phosphorus treated MoO<sub>3</sub> electrodes (marked as MoO<sub>3</sub>/P) is shown in Fig. 4. As can be seen, the MoO<sub>3</sub>/P electrode delivers a capacity of 250 mA h g<sup>-1</sup>, and the MoO<sub>3</sub> electrode delivers a capacity of 280 mA h g<sup>-1</sup> at the first cycle. However, the MoO<sub>3</sub>/P electrode shows better rate performance (Fig. 4b), and at a rate of 10C, the MoO<sub>3</sub>/P electrode can deliver a capacity of 40 mA h g<sup>-1</sup>. The improved rate capability of the MoO<sub>3</sub>/P electrode may be due to the oxygen vacancies that are brought about by phosphorus reduction.

In brief, a novel, simple and efficient method is introduced to reduce the transitional metal Ti<sup>4+</sup> to the more conductive Ti<sup>3+</sup> and induce oxygen vacancies in the Li<sub>4</sub>Ti<sub>5</sub>O<sub>12</sub> lattice. Red phosphorus powder is used as a reducing agent due to its sublimation at a relatively low-temperature of 400 °C. XPS, XRD, and EPR characterization results prove the existence of Ti<sup>3+</sup>. The electrochemical performance reveals that the phosphorus treatment improves the capacity, rate, and cycling capability of the LTO electrode. Cyclic voltammetry at different scan rates and EIS results disclose that both Li<sup>+</sup> diffusion and electronic diffusion are enhanced for the LTO/P electrode. Extended experiments on MoO<sub>3</sub> also show a positive result, indicating that phosphorus reduction can be effective for other metal oxide electrode materials. This method requires a relatively lower temperature compared to the reported similar works, which could greatly save production costs and is favorable for the practical applications of the LTO material and even universal use for other metal oxide electrode materials.

This work was supported by the Natural Science Foundation of the Jiangsu Higher Education Institution of China (Grant No. 18KJB150029), the Natural Science Foundation of Jiangsu Province (No. SBK2018042005), the Research Start-up Foundation (No. 331812150) and the Natural Science Foundation (No. XKZ2017006) of Suzhou University of Science and Technology. We also thank the support from the National Science Foundation of United States (Grant No. DMR-1808517). W.-Y. W. acknowledges

the financial support from the Hong Kong Research Grants Council (PolyU 153051/17P), the Hong Kong Polytechnic University (1-ZE1C), and Ms Clarea Au for the Endowed Professorship in Energy (847S).

## Conflicts of interest

There are no conflicts to declare.

## References

- 1 N. Nitta, F. Wu, J. T. Lee and G. Yushin, Mater. Today, 2015, 18, 252-264.
- 2 I. Belharouak, G. M. Koenig and K. Amine, J. Power Sources, 2011, 196, 10344-10350.
- 3 T. F. Yi, L. J. Jiang, J. Shu, C. B. Yue, R. S. Zhu and H. B. Qiao, J. Phys. Chem. Solids, 2010, 71, 1236-1242.
- 4 X. Y. Feng, X. Li, M. Tang, A. Gan and Y.-Y. Hu, J. Power Sources, 2017, 354, 172-178.
- 5 H. G. Jung, J. Kim, B. Scrosati and Y. K. Sun, J. Power Sources, 2011, **196**, 7763-7766.
- 6 H. Zou, X. Liang, X. Feng and H. Xiang, ACS Appl. Mater. Interfaces, 2016, 8, 21407-21416.
- 7 D. Capsoni, M. Bini, V. Massarotti, P. Mustarelli, S. Ferrari, G. Chiodelli, M. C. Mozzati and P. Galinetto, *J. Phys. Chem. C*, 2009, **113**, 19664–19671.
- 8 X. Zhang, H. Tian, X. Wang, G. Xue, Z. Tian, J. Zhang, S. Yuan, T. Yu and Z. Zou, Mater. Lett., 2013, 100, 51-53.
- 9 X. Feng, H. Zou, H. Xiang, X. Guo, T. Zhou, Y. Wu, W. Xu, P. Yan, C. Wang, J.-G. Zhang and Y. Yu, ACS Appl. Mater. Interfaces, 2016, 8,
- 10 X. Feng, C. Shen, N. Ding and C. Chen, J. Mater. Chem., 2012, 22, 20861-20865.
- 11 X. Feng, N. Ding, Y. Dong, C. Chen and Z. Liu, J. Mater. Chem. A, 2013, 1, 15310-15315.
- 12 Q. Zhang, C. Zhang, B. Li, D. Jiang, S. Kang, X. Li and Y. Wang, Electrochim. Acta, 2013, 107, 139-146.
- 13 Q. Zhang, C. Zhang, B. Li, S. Kang, X. Li and Y. Wang, Electrochim. Acta, 2013, 98, 146-152.
- 14 T. F. Yi, Y. Xie, L. J. Jiang, J. Shu, C. B. Yue, A. N. Zhou and M. F. Ye, RSC Adv., 2012, 2, 3541.
- 15 S. Huang, Z. Wen, X. Zhu and Z. Gu, Electrochem. Commun., 2004, 6, 1093-1097
- 16 C. Lin, M. O. Lai, L. Lu, H. Zhou and Y. Xin, J. Power Sources, 2013, 244, 272-279.
- 17 W. Wang, H. Wang, S. Wang, Y. Hu, Q. Tian and S. Jiao, J. Power Sources, 2013, 228, 244-249.
- 18 C. Zhang, D. Shao, J. Yu, L. Zhang, X. Huang, D. Xu and X. Yu, J. Electroanal. Chem., 2016, 776, 188-192.
- 19 M. R. Jo, K. M. Nam, Y. Lee, K. Song, J. T. Park and Y.-M. Kang, Chem. Commun., 2011, 47, 11474-11476.
- 20 L. Wen, G. Liu, G.-Y. Liu, G.-Q. Liu, F. Lia and H.-M. Cheng, J. Chin. Chem. Soc., 2012, 59, 1201-1205.
- 21 Y. Shiraishi, N. Saito and T. Hirai, J. Am. Chem. Soc., 2005, 127,
- 8304-8306 22 K. K. Mandari, A. K. R. Police, J. Y. Do, M. Kang and C. Byon,
- Int. J. Hydrogen Energy, 2018, 43, 2073-2082. 23 Y. Liu, R. Xiao, Y. Fang and P. Zhang, Electrochim. Acta, 2016, 211,
- 1041-1047. 24 C. Qiu, Z. Yuan, L. Liu, S. Cheng and J. Liu, Chin. J. Chem., 2013, 31, 819-825.
- 25 J. Wang, Z. Yang, W. Li, X. Zhong, L. Gu and Y. Yu, J. Power Sources, 2014, 266, 323-331.